UDC 666.972:539.421.2

# THE STRUCTURE OF CEMENT MATERIALS BY THE METHOD OF NANOINDENTATION

***E. N. Polonina[1], S. N. Leonovich[1,2], O. Lahayne[3], J. Eberhardsteiner[3], V. V. Potapov[4], S. A. Zhdanok[5]***

*[1] Belarusian National Technical University, Minsk, grushevskay_en@tut.by*
*[2] Qingdao University of Technology, China, Qingdao*
*[3] Vienna University of Technology, Austria, Vienna*
*[4] Research Geotechnological Center, Far Eastern Branch of the Russian Academy of Sciences, Russia, Petropavlovsk-Kamchatsky*
*[5] Advanced research and technology, Belarus, Minsk*

**Abstract**

The parameters of the nanoindentation method were selected to ensure the final consistent results were obtained. These results are presented by histograms of the distribution of nanoindentation points by elasticity and hardness moduli and distributions by these characteristics in the horizontal XY plane perpendicular to the movement of the nanoindenter. It was revealed that the elastic modulus increases in samples that contain a complex additive containing nano-sized particles. The effect is also observed when introducing an additive containing only one type of nanoparticles (hydrothermal $SiO_2$ nanoparticles or multiwalled carbon nanotubes MWCNTs. Studies of cement stone samples at W/C = 0,21 and the content of $SiO_2$ in the combined additive is 0,000006 wt. % and MWCNT 0,00004 wt. % for cement showed that the effect of nanoparticles on the structure of the CSH gel becomes more pronounced, because the volume fraction of the LD phase of the CSH gel with a low packing density of nanograins becomes significantly lower than the fraction of the HD phase with an increased hexagonal packing density of granules. The results obtained indicate that there is a change in the nanostructure of the C –S –H gel, which is compared with an increase in strength, Young's and shear moduli with the introduction of $SiO_2$ nanoparticles and MWCNT nanoparticles. Using the nanoindentation method, it becomes possible to explain the nanogranular nature of the CSH gel, which is characteristic and determined by the contact forces of the CSH gel particles for these phases.

**Keywords:** nanoparticles, nanoindentation, nanogranules, packing density.

Analysis of scanning electron microscope (SEM) images of sections of cement stone (Figure 1 a–d) proves the absence of adhesion of $SiO_2$ and MWCNT nanoparticles, as well as their complex (SP + $SiO_2$ + MWCNT) in the hardening sample.

The results of our own studies of heavy concrete samples [9] using a complex nanodisperse system (containing a superplasticizer additive SP + $SiO_2$ + MWCNTs) for compressive strength *fc* at the age of 28 days reached 78,7 MPa, which exceeds the strength of the control sample by more than 50 % and the strength of the sample containing only a superplasticizer by 37 %. The difference in compressive strength fc was also established *between* control sample No. 1 and modified samples No. 2, 3, 4.

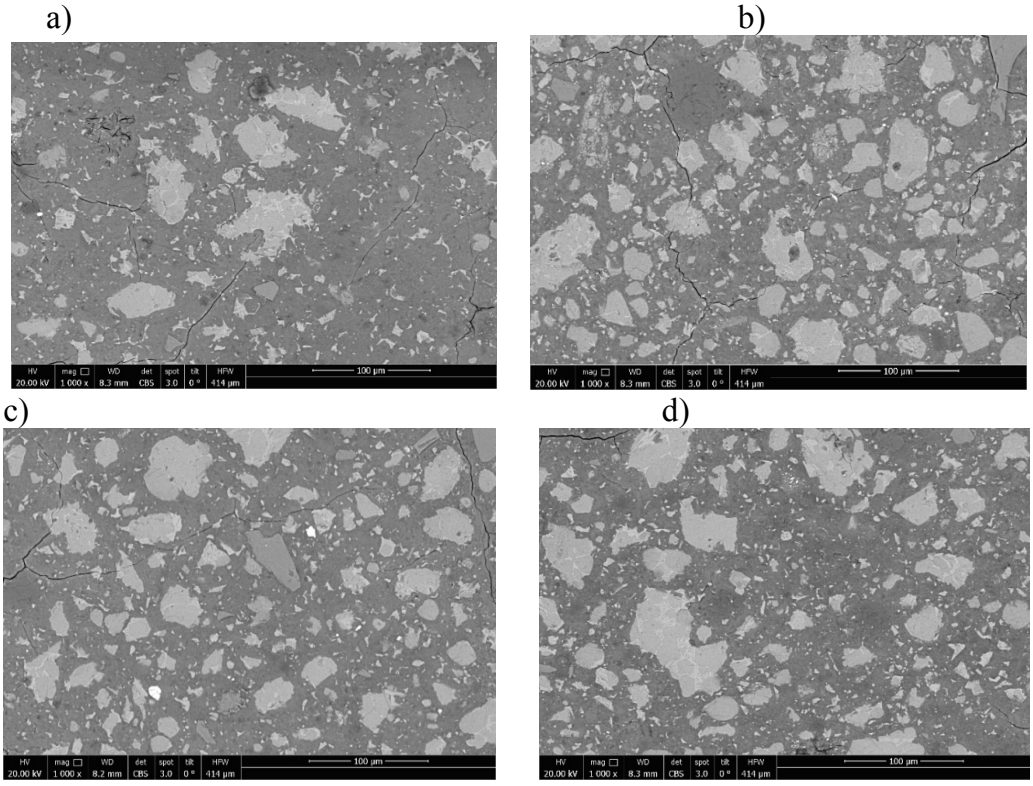


**a) a sample containing only SP (composition No. 1);**
**b) a sample containing SP+ $SiO_2$ (composition No. 2);**
**c) a sample containing SP + MWCNTs (composition No. 3);**
**d) sample containing SP + $SiO_2$ + MWCNTs (composition No. 4)**
***Figure 1*** *– SEM images*

The difference reached 13 and 12,7 % at an early age of 1, 3 days, 11,9 % at the age of 37 days and was maximum in the case $_{of}$ combinations of nanoparticles ($SiO_2$ + MCNT). The difference in bending strength *f* with t relative to the control was maximum for the sample with the complex addition of NPs ($SiO_2$ + M CNTs) and reached 39,6 and 21,6 % at the age of 1,3 days, and 23,4 % at the age of 37 days.

Based on the results of ultrasonic measurements, significant increases in Young's modulus *E* and shear modulus *G* at the age of 1 and 5 months were obtained for samples modified with nanoparticles. The maximum increment of 10 % was achieved in the variant of modification with a complex nanoadditive (sample No. 4). An increase in density *ρ*additionally indicates a change in the pore structure of the cement stone and the structure of the C S H gel (Figure 2). Nanoindentation primarily shows differences in structure, and such significant differences between samples with nanoparticles No. 2, 3, 4 and sample No. 1 without nanoparticles have already been identified, and these differences must be attributed to the action of nanoparticles.

*Test method.* To implement the nanoindentation experiment, the manufactured samples were ground on a single-disc grinding and polishing machine. Grinding was carried out in order to reduce the surface roughness of the test sample and thus reduce its influence on the final indentation results (Figure 3). The polishing surfaces were subsequently photographed using atomic force microscopy (AFM). The roughness turned out to be about 12–25 nm.

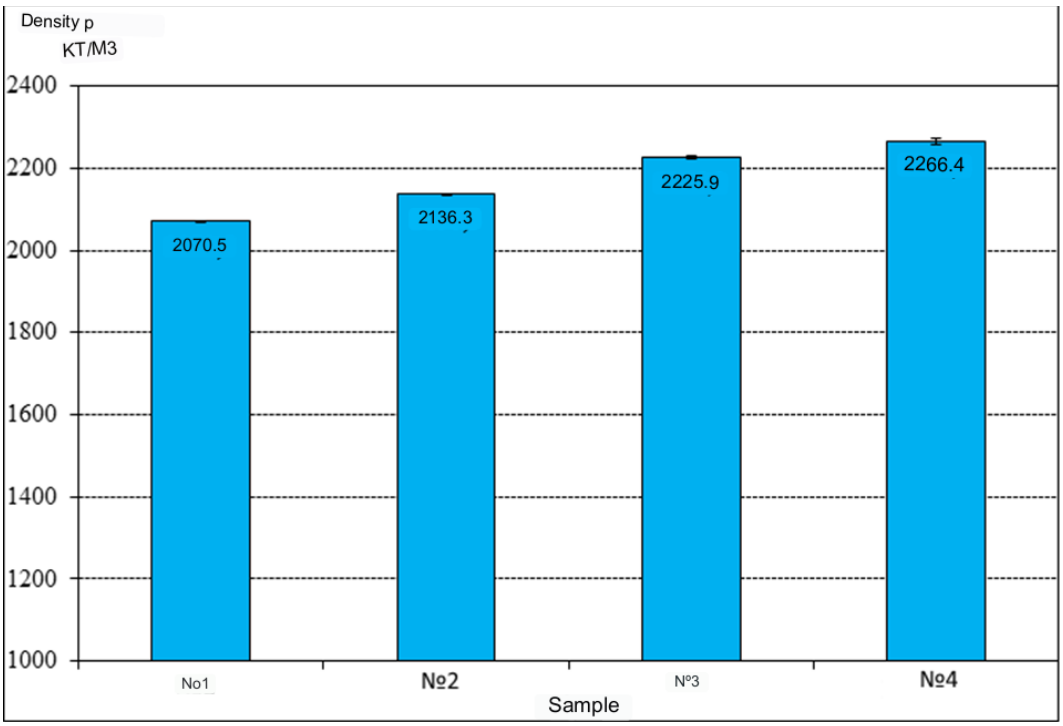


***Figure 2*** *– Results of determining the density of samples*

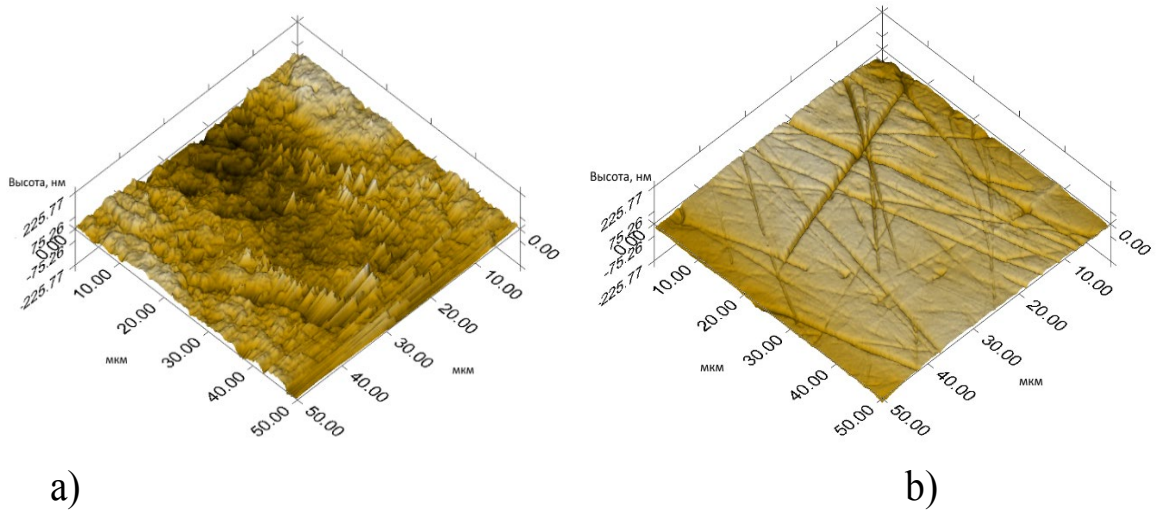


a) b)

***a*) before grinding; *b*) after grinding**
***Figure 3*** *– AFM photographs*

The results of the experiments were histograms of the distribution of nanoindentation points of the mechanical properties of the material-elastic modulus M and hardness H. They were determined by a large number of nanoindentation experiments at a given scale of observation of the material, taking into account the depth of indentation. In this regard, the issue of the immersion depth of the nanoindenter was separately studied. The size of inhomogeneities in the CHS gel structure is 5, 10 and 60 nm, with the maximum size of inhomogeneity being 60 nm. A 5-fold margin was adopted to distinguish heterogeneity, then the maximum immersion depth of the nanoindenter was 300 nm, the maximum load was 4 mN. For

an immersion depth of 200 nm, 1–2 mN is usually sufficient, however, taking into account that the samples had a compressive strength 2 times greater than normal, a maximum force of 4 mN was taken for an immersion depth of 300 nm. If the nanoindenter fell into a crack, then such points were simply excluded from mathematical processing, but the progress of the nanoindenter along the mesh did not stop. The percentage of such points with cracks was no more than 5 %.

In accordance with the direction of the research, a targeted time schedule of the load was specially developed: 1. immersion up to 300 nm and maximum force for 10 s; 2. constant load mode for 5 s; 3. raising the nanoindenter to the surface, removing the load to 0 for 10 s. When choosing the immersion rate of the nanoindenter, simple calculations were performed. We assume the maximum immersion depth of the nanoindenter is 300 nm, the immersion time is 10 s, then the immersion speed will be 300 nm / 10 s = 30 nm / s.

Features of the experiment:

1) type of nanoindenter used with a Berkovich tip with a cone angle of 143 degrees;

2) in a single test (immersion –reaching the surface) we obtain two standard force – immersion depth curves for loading and unloading;

3) based on the maximum load and contact area of the nanoindenter with the sample, hardness *H is calculated*;

4) Using the tangent of the tangent to the unloading curve at the top point, the elastic modulus *E* at one point is calculated.

– unloading" cycle, a P–h diagram of the dependence of the load on the indenter penetration depth was built and saved (Figure 4).

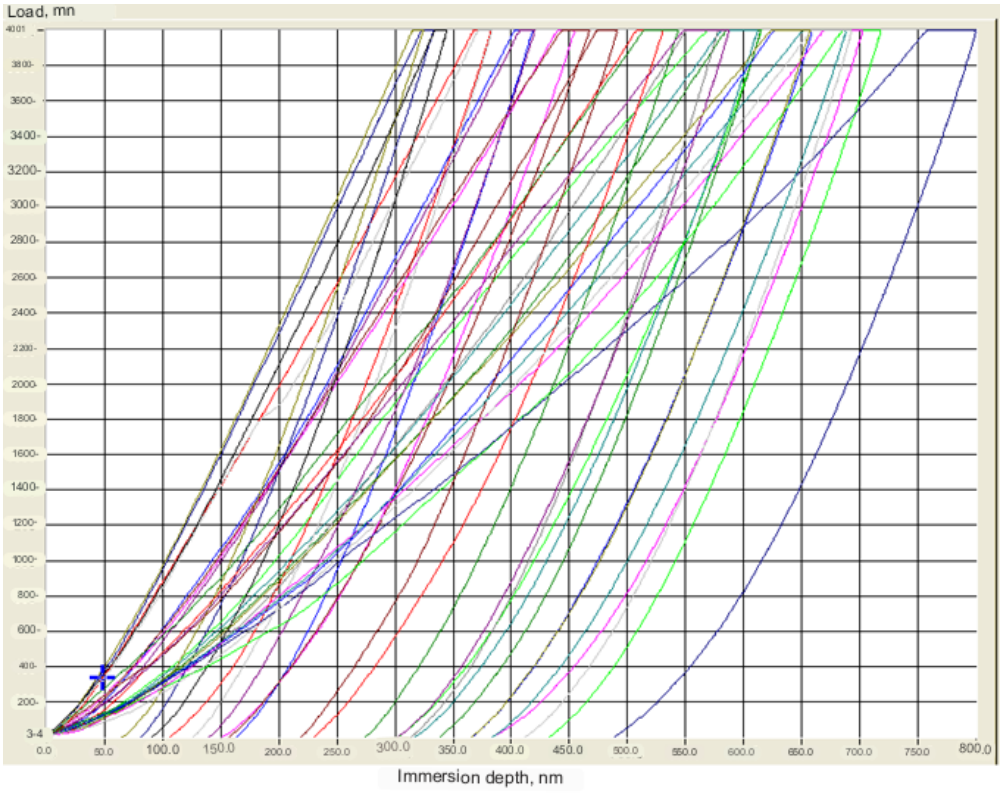


***Figure 4*** *– Hysteresis curves during nanoindentation*

*M* were calculated at the indentation point; from the maximum load and area of the contact zone, *H was calculated.*

Using the calculated values of *M* and *H,* distributions were constructed depending on the contact depth of immersion (Figure 5), from the distributions we proceeded to histograms of *M* and *H* by intervals.

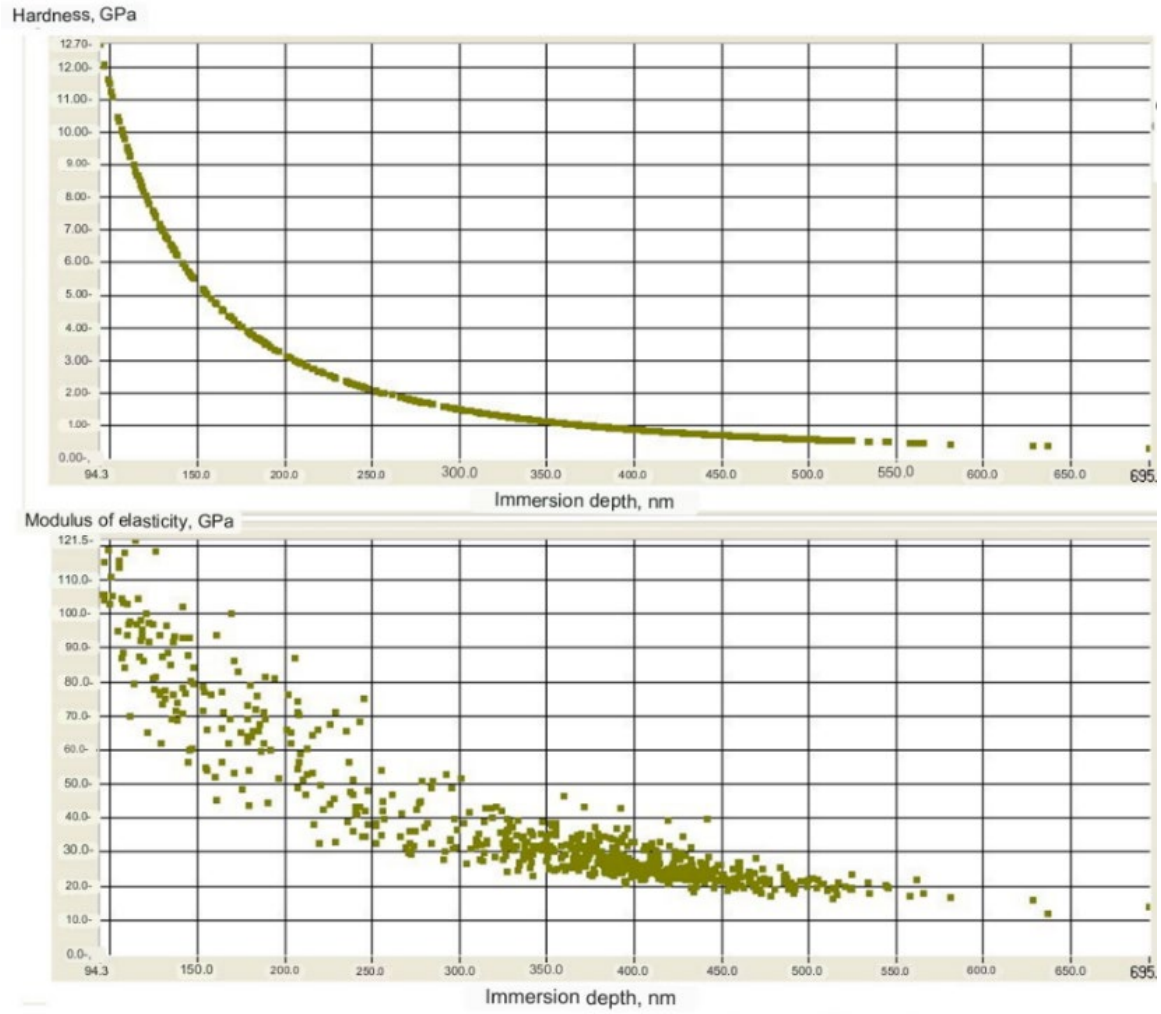


***Figure 5*** *– Distributions of H and M values depending on the contact depth of immersion*

Based on equations (13) and (14), Gaussian functions were found and deconvolution was carried out over three phases (Figure 6).

Designations in the figures: circles (or dots) – experimental measured values of M, H; 2) three dotted lines – the values of three Gaussian functions based on the results of deconvolution; 3) solid blue line – the sum of the values of three Gaussian functions.

Taking into account the rectangular shape of the grid of nanoindentation points in *XY coordinates* (17–35 points) and the distance between grid points of 0.5 mm = 500 μm, × the distributions of *M* and *H in one horizontal plane* were obtained by linear approximation of the values of *M* and *H* along the lines between the grid nodes and for points on the area squares 0,5 × 0,5 mm with corners at grid nodes (Figure 7).

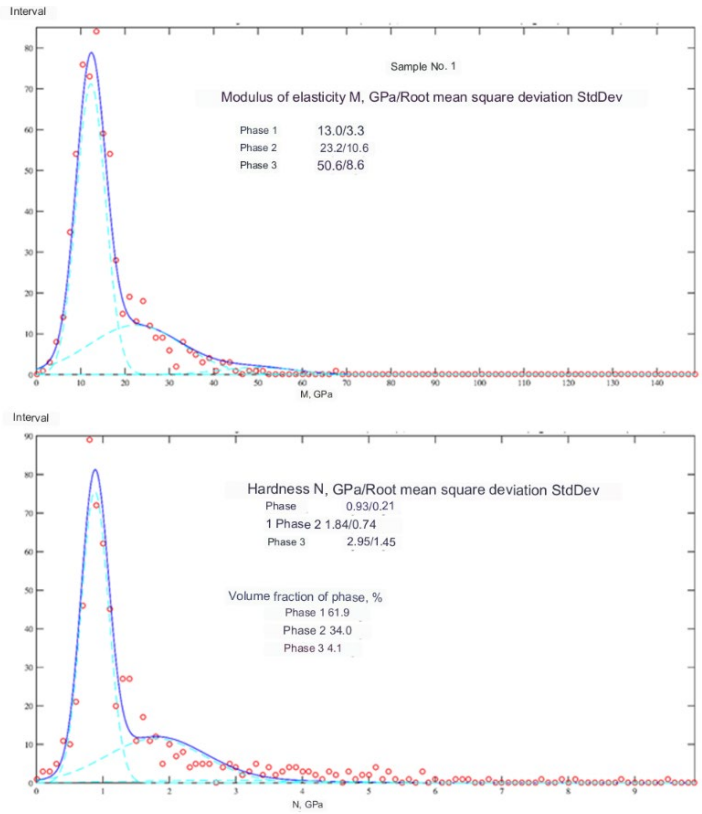


***Figure 6*** *– Histogram of distribution of nanoindentation points by elastic modulus E and hardness H for sample No. 1*

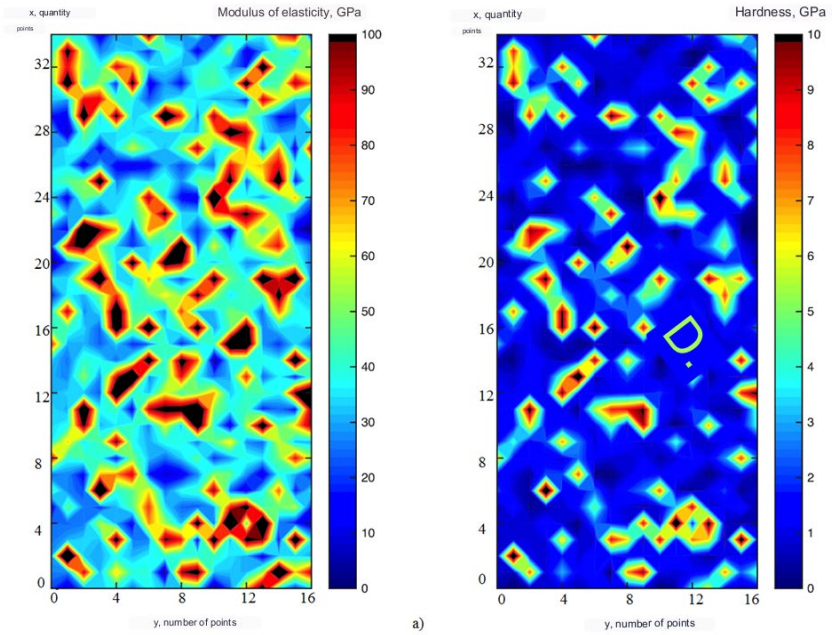


***Figure 7*** *– Distributions of M and H in the horizontal XY plane perpendicular to the movement of the nanoindenter: sample No. 1*

**Analysis of the results obtained.** Results of deconvolution of histograms of volume distribution according to the reduced modulus of elasticity M and stiffness in three phases – exponential Gaussian functions. The values of hardness, Young's modulus and phase fraction for cement samples are presented in Table 1.

**Table 1** – Values of hardness, Young's modulus and phase fraction for cement samples

| Index | | Sample No. 1 | Sample No. 2 | Sample No. 3 | Sample No. 4 |
|---|---|---|---|---|---|
| Modulus of elasticity M , GPa/ Standard deviation StdDev | Phase 1 | 13,0/3,3 | 27,6/4,8 | 21,2/4,9 | 22,6/5,7 |
| | Phase 2 | 23,2/10,6 | 41,7/11,8 | 30,7/9,1 | 36,8/13,4 |
| | Phase 3 | 50,6/8,6 | 90,7/14,6 | 62,8/10,7 | 61,7/15,4 |
| Hardness N , GPa/ Standard deviation StdDev | Phase 1 | 0,93/0,21 | 1,01/0,23 | 1,04/0,23 | 0,90/0,22 |
| | Phase 2 | 1,84/0,74 | 1,57/0,74 | 1,59/0,87 | 1,43/0,62 |
| | Phase 3 | 2,95/1,45 | 2,81/1,37 | 4,94/1,28 | 4,18/1,29 |
| Phase fraction, % | Phase 1 | 61,9 | 58,0 | 46,9 | 55,6 |
| | Phase 2 | 34,0 | 29,2 | 44,1 | 31,4 |
| | Phase 3 | 4,1 | 12,8 | 9,0 | 13,0 |

The histograms highlight phases with average values of *E* and *H* and moderate statistical scatters within each phase. The share of each phase was estimated as a percentage.

Procedure for approximation by Gaussian functions: start parameters and number of phases are set *n, and the* Matlab program selects the averages *M* and *H*, average deviations for each phase, and volume fractions of phases from the condition of the minimum sum of squared deviations between experimental and theoretical points.

The results obtained show that the histograms of volume distribution according to the reduced modulus of elasticity M and stiffness H in samples 2, 3, 4 shifted to the region of higher average values compared to sample 1 (Table 1). At the same time, the volume fraction of phase 1 with lower average values of M and H decreased, and the volume fraction of phases 2 and 3 with larger average values of M and H and with a denser volumetric packing of CSH gel particles increased.

For phases 1, 2, 3 of the distribution over $M_{avg}$ , for phase 3, which has the maximum average value $H_{avg}$ of the distribution over H in samples 2, 3, 4, the width of the distribution according to the corresponding Gaussian function decreased, which is characterized by a decrease in the ratio StdDev / $M_{avg}$ , $H_{avg}$ ( StdDev is an exponent of the Gaussian function), and shows a higher structural order of the CSH gel in samples modified with nanoparticles (Table 2). The data presented in Table 2 indicate a change in the structure of the CSH gel in samples modified with $SiO_2$ nanoparticles and MWCNTs.

**Table 2** – Relative values of the Gaussian function

| Relative values | | Sample No. 1 | Sample No. 2 | Sample No. 3 | Sample No. 4 |
|---|---|---|---|---|---|
| StdDev / M avg | Phase 1 | 0,226 | 0,174 | 0,231 | 0,252 |
| | Phase 2 | 0,457 | 0,283 | 0,296 | 0,364 |
| | Phase 3 | 0,170 | 0,161 | 0,170 | 0,250 |
| StdDev /Hcp | Phase 1 | 0,226 | 0,228 | 0,221 | 0,244 |
| | Phase 2 | 0,402 | 0,471 | 0,547 | 0,434 |
| | Phase 3 | 0,492 | 0,488 | 0,259 | 0,309 |

The average values of the elastic modulus M and stiffness H, calculated as the sum of the products of the average value of M, H in each phase and its volume fraction, for samples of compositions No. 1–4 had the following values: 1–18,00 GPa, 1,32 GPa; 2–39,79 GPa, 1,40 GPa; 3–29,13 GPa, 1,14 GPa; 4–32,14, 1,49 GPa. The volume-average values of M, H in samples of compositions No. 1–4, modified with nanoparticles, were higher than in the sample of composition No. 1.

The nanoindentation method, a significant shift in the volume fraction of the CSH gel phases to the region of higher average values of M and H and a decrease in the StDev / M, H ratio for the isolated phases were established, which indicates a higher packing density of the gel particles, a higher structuring of the gel substance, and can be correlated with the differences characteristics ($E$ , $G$ , $\rho$, $f_c$ , $f_{ct}$) [14].

The nanoindentation results suggest that the two packing limits that characterize LD CSH and HD CSH are a consequence of the nanogranular nature of CSH. Nanogranular nature refers to the nanoscale mechanical behavior of CSH particles, which is dominated by particle-particle contact rather than mineral properties. As the packing density increases, the number of contacts increases. Thus, the higher stiffness and hardness of HD CSH compared to LD CSH is attributed to the large number of contact points that stabilize the particle.

**Conclusions**

1. CSH is improved due to the high specific surface area and specific surface energy of $SiO_{2\ nanoparticles}$ and carbon nanoparticles. The surface of nanoparticles acts as additional centers of crystallization of calcium hydrosilicate particles, helping to increase the rate of alite hydration and formation of CSH gel, reducing the average size and increasing the volumetric packing density of particles and mechanical characteristics in the CSH gel phases, increasing the structural order in the CSH gel phases and in the particles of calcium hydrosilicates. The consequence of nanomodification is changes in the structure of the CSH gel:

2. Hysteresis curves were obtained for the points of the indentation grid (Figure 6). For all grid points, the curves were smooth and continuous of a similar shape, which made it possible to calculate arrays of *M* and *H values* and proceed to the distributions of *M* and *H* depending on the contact depth of immersion

3. The shift to the region of higher average values indicates an increase in the volume fraction of C – S – H gel phases with a higher particle packing density and, accordingly, higher mechanical characteristics. The increase in the volume fraction of the C – S – H phases of the gel with higher *M* and *H values* is consistent with the results of an increase in the strength, Young and shear moduli, and density of samples modified with $SiO_2$ nanoparticles and MWCNTs.

4. The volume fraction of the phase with increased values of *M* (more than 70–100 – GPa) and *H* (–5–10 GPa) according to nanoindentation data (the relative area of the red, brown and black areas), which can be compared to non-hydrated clinker grains, has low values in samples No. 1–4, corresponding to the degree of hydration of Portland cement with a W/C ratio = 0,21 at the age of 3 months.

5. Based on the results of nanoindentation, we can conclude that CSH gel behaves mechanically like a nanogranular material, the behavior of which is determined by contact forces at the points of contact of particle with particle, and not by the mineral properties themselves.

## References


1. Sanchez, F. Nanotechnologies in the production of concrete. Review / F. Sanchez, K. Sobolev // Bulletin of Tomsk State Architecture and Construction university. – 2013. – No. 3 (40). – P. 262–289.

2. Ulm, F. J. Nano-Engineering of Concrete / F. J. Ulm // Arabian Journal for Science and Engineering. – 2012. – Vol. 37, no. 2. – P. 481–488.

3. Constantinides, G. The nanogranular nature of C–S–H / G. Constantinides, F. J. Ulm // J. Mechanics Phys. Solids. – 2007. – Vol. 55, Issue 1. – P. 64–90.

4. Investigation by atomic force microscopy of forces at the origin of cement cohesion / S. Lesko [et al.] // Ultramicroscopy. – 2001. – Vol. 86, Issue 1–2. – P. 11–21.

5. Study of C–S–H growth on $C_3S$ surface during its early hydration / S. Garrault [et al.] // Materials and Structures. – 2005. – Vol. 38, Issue 4. – P. 435–442.

6. Investigation of the surface structure and elastic properties of calcium silicate hydrates at the nanoscale / S. Plassard [et al.] // Ultramicroscopy. – 2004. – Vol. 100, Issue 3–4. – P. 331–338.

7. Preparation of a complex additive for increasing the strength of concrete based on nanodispersed silicon dioxide of hydrothermal solutions / V. V. Potapov [et al.] // Fundamental research. – 2012. – No. 9–2. – P. 404–409.

8. Quantification and characterization of C –S –H in silica nanoparticles incorporated cementitious system / L. P. Singh [et al.] // Cement & Concrete Composites. – 2017. – Vol. 79. – P. 106–116.

9. Modification of Cement Concrete by Admixtures Containing Nanosized Materials / S. A. Zhdanok [et al.] // Journal of Engineering Physics and Thermophysics. – 2020. – Vol. 93, no. 3. – P. 669–673.

11. Elastic Properties of Calcium Silicate Hydrates by Nanoindentation / S. Plassard [et al.] // 12th International Congress on the Chemistry of Cement. – Montreal : Canada, 2007. – P. 44.

12. Microscopic physical basis of the poromechanical behavior of cement-based materials / A. Gmira [et al.] // Materials and Structures. – 2004. – Vol. 37, no. 265. – P. 3–14.

13. Nanoindentation method for studying the structure of modified cement stone / E. N. Polonina [et al.] // Journal of Engineering Physics and Thermophysics. – 2021. – Vol. 94, no. 5. – P. 1194–1207.

14. Mechanism for Improving the Strength of a Cement Material Modified by $SiO_2$ Nanoparticles and Multiwall Carbon Nanotubes / E. N. Polonina [et al.] // Journal of Engineering Physics and Thermophysics. – 2021. – Vol. 94, no. 1. – P. 67–78.

15. Studying the Structure of a Cement Composite Modified by Hydrothermal $SiO_2$ Nanoparticles and MCNTs by the IR-Spectroscopy Method / E. N. Polonina [et al.] // Journal of Engineering Physics and Thermophysics. – 2022. – Vol. 95, no. 6. – P. 1426–1436.

16. Investigation of the Structure of a Cement Composite Modified by Hydrothermal SiO2 Nanoparticles and MCNT Nanoparticles by the X-Ray Phase Analysis Method / E. N. Polonina [et al.] // Journal of Engineering Physics and Thermophysics. – 2023. – Vol. 96, no. 1. – P. 215–223.